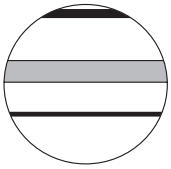

The Holocene
1–17

DOI: 10.1177/09596836221121761
journals.sagepub.com/home/hol
SAGE

Expanded agroecological niches and redistributed risks in northern Peru's Chicama Valley during late-Holocene ENSO climate changes

Benjamin R Vining,[1] Aubrey Hillman,[2] Daniel A Contreras[3] and Ernesto Tejedor[2]

Abstract

South American arid lands present unique constellations of climatic risk to their human inhabitants, due to volatile events that can create markedly different hydroclimate conditions over interannual–centennial scales. However, a main driver of such volatility – the El Niño/Southern Oscillation (ENSO) – occurs with semiregular periodicity. Paleoclimatic and archeological evidence indicate not only that the strength and periodicity of ENSO patterns have changed over the late-Holocene, but their impacts were likely recognized, adapted to, and perhaps capitalized upon by agriculturalists employing adaptive risk strategies. We examine relationships over the last 1.3 kyr between ENSO periodicity, ecological transitions, and archeological settlement in Peru's Chicama Valley through a coupled paleohydroclimate and agroecology model. We reconstruct periods when ENSO-like conditions dominated past hydroclimates and present a quantitative, spatially-explicit analysis of ecological productivity during modern ENSO-positive hydroclimate conditions. We show that archeological settlement patterns are sensitive to these transformations and reflect efforts to capitalize on expanded agroecological niches. Such expanded niches potentially offset the adverse impacts and risks associated with abrupt ENSO climate events. These results suggest archeological communities were aware of ENSO risk and managed productive strategies accordingly, highlighting the importance of a risk calculus that considers the *net* ecological effects of climate events.

Keywords

agroecological modeling, archeological settlement patterns, climate change, climate risk, el Nino Southern Oscillation (ENSO), Peru

Received 14 October 2021; revised manuscript accepted 10 May 2022

Introduction: ENSO climate change and risk societies

Abrupt climate changes are typically interpreted as high-risk events, particularly in arid regions where margins between amenable and adverse conditions are narrower and changes in hydroclimate can have high socio-ecological costs. Construing abrupt climate change as risky, however, is predicated on several assumptions. These include assumptions that human systems (built environments and intangible infrastructure) are adapted to relatively static climatic conditions, are relatively inflexible in their design, and consequently were profoundly disrupted by external climatic or environmental changes in state. These characterizations leave little room for adaptive socioecological behaviors that recognized and accounted for inherent climatic/environmental variability, including potential risks that variability might pose.

Current paleoclimatic research emphasizes the non-stationarity of climate change; similarly, climate change anthropology demonstrates that communities are cognizant of "normal" ranges of climatic variability and manage such variability through diverse socio-ecological strategies (e.g. Crate, 2011; Crate and Nuttall, 2016; Hudson et al., 2012). While complex socio-climate models accommodate ideas about vulnerability and resilience, they continue to largely construe climate risk as an externality.

An alternative to such paradigms is the "risk society" perspective (Beck and Wynne, 1992; Ekberg, 2007; Giddens, 1999). While originally applied to modern industrial socio-environmental issues, the risk society concept has tenets applicable to Holocene socio-climatic dynamics. It proposes that risk is not wholly external (i.e. caused solely by physical factors) but is partially constituted by – and knowingly assumed within – the environmental decisions people collectively make. Societies construct individual and systemic risk through dependencies on physical (technological) and behavioral (sociopolitical) infrastructure, creating vulnerabilities. Societies develop a reflexive risk-awareness, including, critically, a willingness to assume certain amounts of risk as a function of a probabilistic calculus. Importantly, risk

[1]Department of Anthropology and Environmental Dynamics, University of Arkansas-Fayetteville, USA
[2]Department of Atmospheric and Environmental Sciences, University at Albany-SUNY, USA
[3]Department of Anthropology, University of Florida, USA

Corresponding author:
Benjamin R Vining, Department of Anthropology and Environmental Dynamics, University of Arkansas-Fayetteville, 330 Main, Arkansas, AR 72701, USA.
Email: bvining@bu.edu

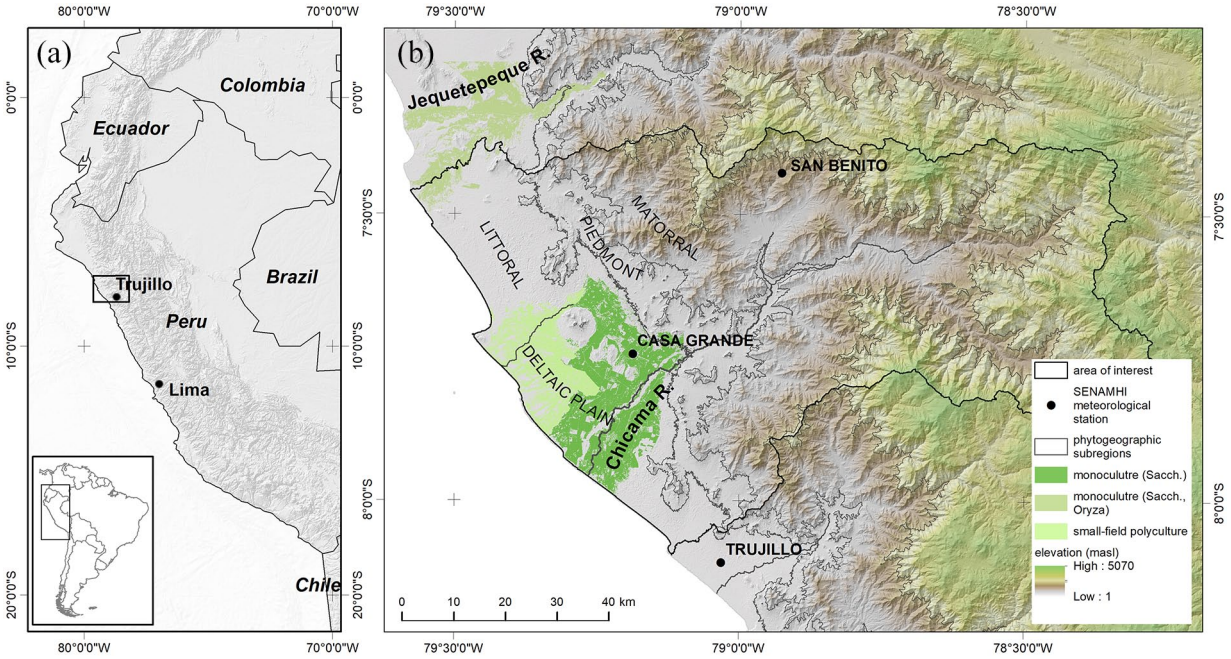

Figure 1. (a) Index map of the study region in NW South America. (b) Map of the Chicama River area of interest, with phytogeographic subregions and meteorological stations used in this analysis indicated.

is not necessarily assumed evenly by all members of a community but distributed across its social segments.

The Central Andean region (between approximately 5° – 30° S latitude) includes environmental extremes – hyper-arid coastal deserts, high elevation steppes, and lowland neotropical rainforests – as well as hydroclimatic variability driven by the South American Summer Monsoon (SASM) and El Niño Southern Oscillation (ENSO, Figures 1 and 2). Because of these dynamics, human – environmental interactions within the region frequently are characterized as high-risk. The literature on ENSO generally embraces this model, construing ENSO phases (particularly positive phases or "el Niños," hereafter abbreviated as ENSO+) as volatile departures from "normal" hydroclimate conditions that posed catastrophic risk to agriculture-dependent subsistence and political economies (Billman and Huckleberry, 2008; Moseley et al., 2008; Nesbitt, 2016; Sandweiss and Quilter, 2008; Sandweiss et al., 2007).

Here, we present a coupled climate-agroecology model that examines how late-Holocene societies in the Chicama Valley of northern Peru situated ENSO-driven climatic risk within a suite of adaptive strategies. A "risk society" perspective suggests that it is important to ask:

(1) Were ENSO+ effects an expected feature of the environment, or a perturbation of the expected/natural order?
(2) In what ways were the effects of ENSO+ phases experienced, adapted to, and even potentially planned for? Were these effects evenly distributed across populations?

We address these questions through fine-grained, spatially-explicit analyses of modern ENSO+ effects as analogs for paleo-ENSO conditions. We evaluate ecological changes during a recent ENSO+ event against agricultural requirements, to examine the spatio-temporal limits of ENSO-driven risk and how these may have been offset by beneficial circumstances. This model is coupled with high resolution reconstructions of late-Holocene ENSO activity to identify periods of greater and lesser ENSO+ frequency. Spatial models of ENSO effects allow us to leverage archeological settlement data as a proxy for behavioral responses to (or even anticipation of) agroecological changes during ENSO+ periods.

This coupled model allows us to assess whether past inhabitants of the Chicama Valley responded to environmental changes during late-Holocene ENSO+ conditions by managing alternative agroecological strategies. These dynamics suggest that risk awareness and mitigating the disastrous effects of abrupt climate events was critical to the development of socio-politically complex agricultural societies in the drylands of NW South America over the past 1.3 kyr. The ability of these societies to recognize and mitigate arid-lands risk can provide key insights into past adaptability and inform future resilience efforts.

Context and problem

Geographic and environmental context

Our study region is a neotropical desert on NW South America's Pacific Coast and encompasses the Chicama River Valley and adjacent arid uplands (Figure 1), between 7.25°–8.25° S and 79.75°–79.0° W. Elevations within our study region range from sea level to ~2500 m above mean sea level (m asl). Within this, there are two physiographic environments: the Chicama River deltaic plain and fluvial zone and the incised valleys of the Andean forearc, which here is a granitic coastal cordillera. Edaphic conditions vary greatly, with relatively developed regosols on the deltaic/fluvial regions and poorly formed xerosols and leptosols in uplands (ONERN, 1973). These coastal/alluvial plains constitute oases in an otherwise desert coast. Modern land use is concentrated within these areas and includes low-density rural and urban areas, small-scale polyculture, and intensive industrial monocropping.

Archeological context

Extensive archeological excavation and survey projects document a complex socio- environmental history for Chicama spanning from the late Pleistocene to the historic period (Elera Arévalo, 1998; Bird and Hyslop, 1985; Briceño, 1999, 2011; Caramanica, 2018; Chauchat, 1975; Chauchat et al., 1998; Clément, 2015; Conrad, 1977; Dillehay et al., 2012; Franco et al.,

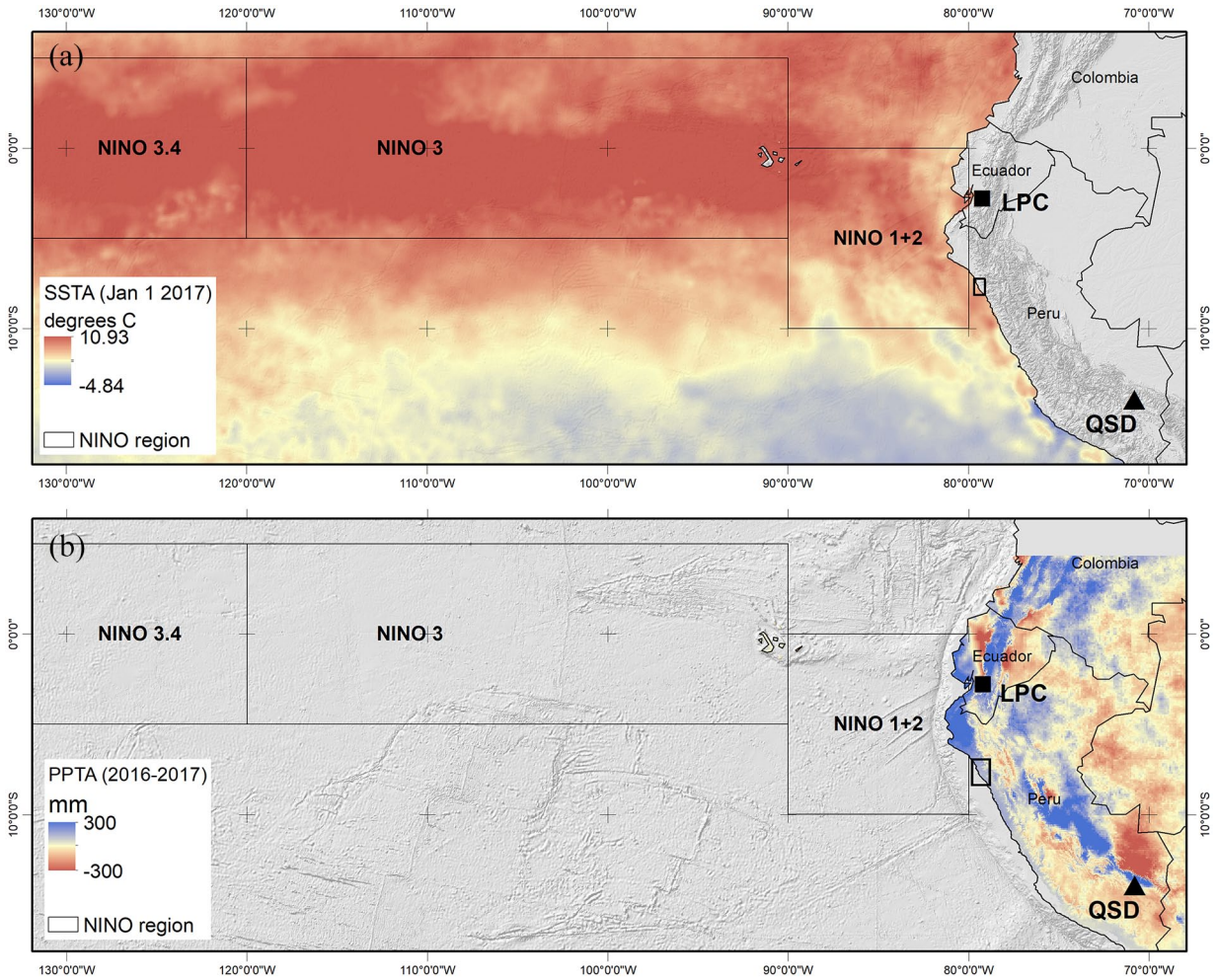

Figure 2. Eastern-central Pacific NINO regions 1–3.4, showing sea surface temperature anomalies (SSTA) that developed during the 2016–2017 ENSO+ phase (a) and total annual precipitation anomalies (PPTA) during the same event (b). The locations of paleoclimate proxy archives mentioned in the text are indicated.
QSD: Quelccaya Summit Dome Ice Core; LPC: Laguna Pallcacocha lacustrine sediment core.

2001; Gálvez Mora and Briceño, 2001; Gálvez Mora and Runcio, 2015; Goodbred et al., 2020; Huckleberry et al., 2018; Koons, 2015; Krzanowski, 1985; Leonard and Glenn, 1992; Netherly, 1984; Shoji, 2018; Toshihara, 2002; Vining, 2018; Watson, 1979).

Our analysis focuses on late-Holocene (the last 1.3 kyr BP) socioclimatic relationships, when well-developed agricultural economies supported large scale and socio-politically complex societies. Agriculture-dependent economies, which relied on anthropogenic planting surfaces and water management systems to make cultivation possible in this hyper-arid region, appeared in Chicama in the mid-Holocene, ca. 3.5 kyr BP (Goodbred et al., 2020). Subsequent societies through the Moche, Chimu, and Colonial eras, ca. 1.8–0.5 kyr BP became more dependent on agricultural production (Billman, 2002; Clément, 2017; Kus, 1975; Watson, 1979).

Prior investigations indicate that two general agricultural strategies were used prehistorically in the Chicama Valley. Most archeological investigations have focused on the valley's floodplain and adjacent low-slope desert margins, where largescale irrigation is viable with relative ease. Well-documented irrigation systems were used to increase plant-available water (PAW) locally and expand cultivable areas (Clément, 2017; Huckleberry et al., 2018; Kus, 1975; Netherly, 1984; Ortloff et al., 1982; Watson, 1979). This evidence, combined with a lack of significant modern land use in desert areas and the region's general aridity, have contributed to the conventional wisdom that non-riparian zones were largely inhospitable to most productive activities.

However, limited but important research in intervalley regions indicate that prehispanic populations made at least episodic agricultural use of intervalley arid lands, potentially during past ENSO+ events (Caramanica, 2018; Chauchat, 1975; Chauchat et al., 1998; Clément, 2017; Gálvez Mora and Runcio, 2011, 2015). This suggests that arid-land potentials dramatically changed during past hydroclimate changes and challenges us to think more expansively about ENSO-driven ecological dynamics.

Hydroclimate dynamics

Hydroclimate is a strongly limiting ecological factor in NW South America arid regions. Temperatures at these latitudes remain moderate year-round except at high altitudes, making moisture availability the primary control on plant viability. The timing and total accumulation of precipitation vary with the Intertropical Convergence Zone's (ITCZ) northward–southward migrations (Abbott et al., 2003; Bird et al., 2011; Vuille et al., 2012) and are modulated by ENSO dynamics. Under modern ENSO-neutral conditions, meteoric precipitation directly on the study region is rare and hyper-arid to arid conditions prevail. Annual average precipitation measured at Casa Grande (7.75° S, 79.19° W, 145 m asl, within the irrigation agriculture niche) is 21.46 mm/annum for the period 1984–2019. San Benito (7.42° S, 78.92° W, 1317 m asl, and within the potential ENSO-expanded niche) mean precipitation for the period 1964–2019 is 431 mm/annum (see Figures 1 and 3).

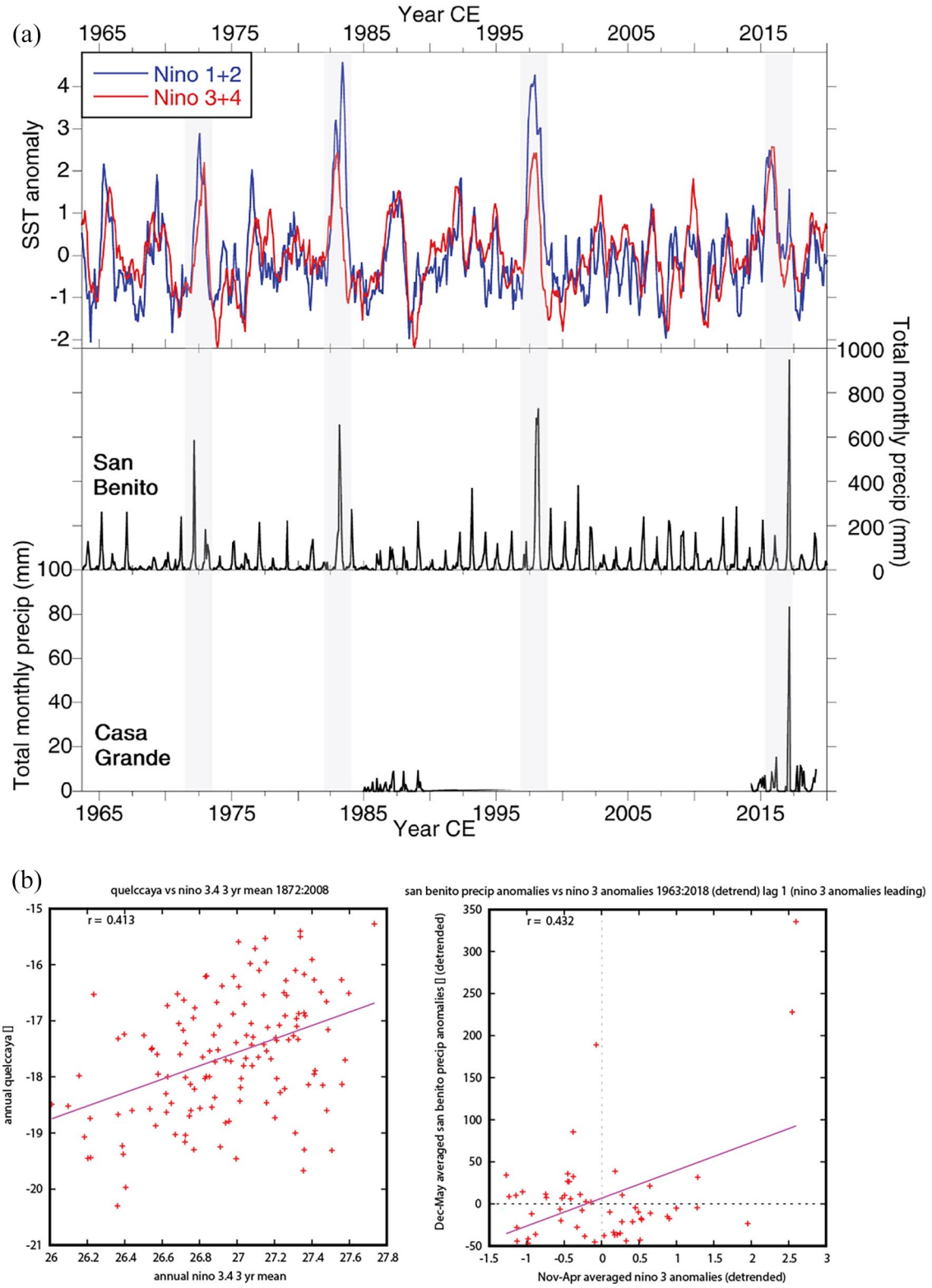

Figure 3. Timeseries for NINO 1.2 and 3.4 sea surface temperature anomalies (SSTA) and monthly pluviometric totals at San Benito and Casa Grande. Button: biplots showing (a) relationships between QSD thermal year δ18O values and NINO 3.4 annual SSTA and (b) departures from mean monthly precipitation recorded at the San Benito SENAMHI pluviometric station and monthly NINO 3 SSTA.

Precipitation occurs mostly as orographic rainfall during the austral summer (December–February, DJF) wet season and is derived from subtropical–tropical easterly Atlantic/Amazonian convective moisture in the SASM pattern (Garreaud, 2009). This moisture enters the study region as surface streams and groundwater as it moves down the Andean slope and across the Pacific coastal plain. Surface and groundwater availability is highly localized, consequently, and largely limited to riparian zones. Orographic factors and the cold Peruvian/Humboldt current inhibit meteoric precipitation from Pacific sources under normal (ENSO-neutral) conditions, although coastal moisture is augmented locally by westerly Pacific coastal fog caused by thermal inversions.

ENSO effects on hydroclimate. While Andean precipitation is derived from Atlantic/Amazonian sources, precipitation patterns

are modulated by ENSO states and other Pacific dynamics (Cai et al., 2020; Garreaud, 2009; Hurley et al., 2019; Vuille and Keimig, 2004). ENSO is a coupled ocean-atmospheric climate phenomenon originating in the equatorial Eastern Pacific (EP, NINO 1 + 2 region) or Central Pacific (CP, NINO 3, 3.4, and 4 regions, see Figure 2). A variety of ENSO patterns have been identified based on their geographical region of development and how this affects ocean-atmosphere dynamics in adjacent regions (Ashok et al., 2007; Cai et al., 2020; Chattopadhyay et al., 2019; Hu et al., 2019; Ramírez and Briones, 2017).

ENSO phases can disrupt the characteristic ENSO-neutral climatic patterns described above. Generally, ENSO+ phases invert ENSO-neutral conditions and bring a weakened Humboldt Current, a deepening Pacific equatorial thermocline, and increased sea surface temperatures (SST) in NINO 1–4 regions (Figure 2). The most salient impacts of ENSO+ conditions for this study are warmer eastern Pacific SST anomalies, which weaken Walker circulation, enhance local coastal and Andean slope precipitation, and decrease precipitation further south and into the Amazonian interior (Bendix, 2000; Cai et al., 2020; Lagos et al., 2008; Rasmusson and Wallace, 1983; Tapley and Waylen, 1990). CP and EP ENSO+ conditions result in spatially slightly different DJF precipitation patterns, particularly in coastal Peru (Cai et al., 2020), but overall patterns are similar. Recent strong ENSO+ events greatly enhanced coastal precipitation early in the March–May (MAM) trimester. The reverse effects occur during ENSO-negative (la Niña) phases.

ENSO is a periodic phenomenon. Under modern conditions, shifts from neutral to ENSO+/− phases develop over approximately 7–12 months and occur irregularly on cycles of 3–7 years. Strong ENSO+/− phases occur with approximate decadal periodicity, with recent severe ENSO+ phases occurring 14–19 years apart (Garcia-Herrera et al., 2008; Gergis and Fowler, 2009; Ortlieb, 2000; Quinn et al., 1987). Recent very strong ENSO+ phases (Multivariate ENSO index ⩾2.0, Zhang et al., 2019) occurred during the austral summers (DJF) of 1972–1973, 1982–1983, 1997–1998, 2015–2016, and 2016–2017 (Figure 3).

Identifying ENSO in paleorecords. From among the well-resolved, Central Andean and equatorial Pacific paleoclimate proxy archives, lacustrine (Moy et al., 2002), tropical ice core (Bradley et al., 2003; Knüsel et al., 2005; Thompson et al., 1984, 2000, 2013), and marine isotopic and microfaunal proxies (Andrus et al., 2002, 2008; Cobb et al., 2013; Koutavas et al., 2006; Woodroffe et al., 2003) have yielded potential Late Glacial Maximum–Holocene paleo-ENSO records. We reconstruct ENSO activity from the Quelccaya Summit Dome (QSD) ice core annual net accumulation (A_n) record (Thompson et al., 1984, 2000, 2013). Both the QSD A_n and $\delta^{18}O$ records are annually-resolved continuous records that cover our period of interest at the greatest temporal resolution. Net accumulation has a clear mechanism linking the proxy record to ENSO activity, with less influence from SASM signals. ENSO and precipitation $\delta^{18}O$ linkages are thought to be due to the influence of ocean-atmosphere dynamics on the equatorial upper-level westerly winds from the Atlantic (Hurley et al., 2019; Vuille and Werner, 2005; Vuille et al., 2003). Enhanced Quelccaya, Illimani, and Sajama $\delta^{18}O$ values and reduced QSD A_n correlate with sea surface temperature anomalies (SSTA) in the NINO3.4 and NINO4 regions (Bradley et al., 2003; Thompson et al., 2000), while ENSO signals are unclear in the Huascaran proxies (Bradley et al., 2003; Knüsel et al., 2005; Thompson et al., 2000). However, the Illimani and Sajama proxy records have lower temporal resolution. Consequently, QSD provides a reliable, high-resolution proxy for paleo-ENSO activity over the past two millennia. Other high-resolution, continuous isotopic records are linked to SASM variability with no discernable paleo-ENSO signal (Abbott et al., 2003; Bird et al., 2011; Kanner et al., 2013; Vuille et al., 2012).

The variety of ENSO conditions (CP vs EP), the complexity of their spatiotemporal development, and chronological vagaries complicates the ability to identify single events. Consequently, ENSO signals across different records are rarely completely coherent, and discrete events may not be captured, particularly across archives. Yet, paleorecords do agree in identifying major decadal- to millennial-scale variability in the strength and periodicity of ENSO activity over the last approximately 3.5 kyr BP (Moy et al., 2002; Rollins et al., 1986; Sandweiss et al., 2007, 2020). As in the QSD A_n and $\delta^{18}O$ record, these signals indicate "ENSO-like precipitation responses" – periods during which regional conditions were more similar to those during ENSO-positive phases, including warmer eastern Pacific SST and enhanced (decreased) precipitation in north-coastal (southern-highland) areas (Thompson et al., 1992: 291, 2013). We use these records to infer periods when hydroclimate conditions resembled those currently seen during ENSO+ events.

ENSO effects on terrestrial ecology and agroecology. Attention to ENSO has been focused on the adverse impacts of ENSO+ phases on marine and coastal plain environments, including marine faunal die-offs; river avulsion; and economic and developmental impacts (Harvell et al., 2002; Kluger et al., 2019; Ñiquen and Bouchon, 2004; Ramírez and Briones, 2017; Ward et al., 2014; Waylen and Caviedes, 1986). Less is known concerning the terrestrial ecological effects of ENSO, including what effect influxes of atmospheric moisture have on PAW and the productivity of various arid-adapted vegetation communities across coastal–matorral ecological zones.

Botanical surveys conducted after recent ENSO+ phases document largely positive or neutral effects of ENSO-enhanced PAW on several arid-adapted botanical communities, with fewer instances of negative impacts (Albán et al., 2006; Cano et al., 1999; Dillon and Rundel, 1990; Eichler and Londoño, 2013; Erdmann et al., 2008; Ferreyra, 1993; Richter, 2005; Tovar et al., 2018; Vining et al., 2022). Vegetation response is not uniform across plant communities, but sensitive to biogeographical, edaphic, orographic, and hydrographic factors (Erdmann et al., 2008; Ferreyra, 1993). While these vegetation communities are not agricultural, their response to ENSO-enhanced moisture does provide a metric from which we can approximate changing ecological potentials during ENSO+ phases.

Modern and pre-modern cultivars used in Chicama are water intensive, and agriculture – past and modern – compensates for limited PAW with surface irrigation systems (see Kus, 1989; ONERN, 1973; Watson, 1979). ENSO-related agroecological risk occurs from excessive amounts of meteoric precipitation that cause flooding and saturation, lost planting surfaces during avulsions, and/or as damages to irrigation infrastructure. Consequently, el Niño events are typically framed as adversely affecting modern (Garnica, 1997) and ancient agricultural productivity (Billman and Huckleberry, 2008; Manners et al., 2007; Moseley et al., 2008). How increased PAW affects irrigated and non-irrigated agricultural potentials, including how it intersects with lost productivity to affect net productivity during and following these climatic events, has not been evaluated.

Methods

Estimating paleo-hydroclimatic conditions during ENSO positive phases

We evaluate relationships between study region hydroclimate and ENSO activity by correlating meteorological data from the Peruvian *Servicio Nacional de Meteorología e Hidrología* (SENAMHI, 2019) with published ENSO SSTA indices (NINO regions 1–4, (Trenberth, 2021)) and the QSD paleo-ENSO record (Thompson

et al., 1984, 2000, 2013). This approach allows us to infer multi-decadal periods during which ENSO frequency and magnitude increased and "ENSO-like precipitation responses" (Thompson et al., 1992: 291) characterized hydroclimatic conditions in the Chicama Valley.

Pluviometric data recorded at the SENAMHI Casa Grande and San Benito stations were downloaded using the R package **senamhiR** (Anderson, 2020). Data were screened for gaps missing more than 2 weeks of consecutive observations. The Casa Grande station was inoperable between September 1989 and March 2013, and these data are not evaluated against NINO SSTA and QSD $\delta^{18}O$. Monthly gaps in San Benito data were filled using a normal-ratio estimation method (Linsley et al., 1988) and concurrent observations from the surrounding SENAMHI stations at Monte Grande, Sinsicap, and Cospan. We used the KNMI Climate Explorer (KNMI-CE, Trouet and Van Oldenborgh, 2013) to evaluate statistical correlations (Pearson's *r*) between pluviometric data, NINO 1+2 – 4 SSTA indices, and thermal-year annual QSD $\delta^{18}O$ (Thompson et al., 2013) values. Precipitation anomalies, calculated as deviations from mean monthly amounts for the period 1964–2020, were uploaded to KNMI-CE, detrended, and compared to detrended monthly NINO SSTA values using mean values for DJF/MAM trimesters. Following Thompson et al. (2013), 3 year running means for QSD $\delta^{18}O$ were calculated and compared to 3 year running mean thermal-year SST in each NINO region.

ENSO-positive conditions are indicated in the QSD record by enhanced $\delta^{18}O$ values relative to the modern (approximately 30 year) average and A_n that is <70% of the modern annual mean (Hurley et al., 2019; Thompson et al., 2013). Decadal-scale mean increases in the QSD $\delta^{18}O$ and decreased QSD A_n reflect periods of prolonged "ENSO-like precipitation responses" (Thompson et al., 1992: 291, 2013). These should not be understood as identifying individual ENSO events, but rather decadal-scale periods during which oceanic-atmospheric conditions and hence hydroclimate more closely resembled those during modern ENSO+ phases.

To identify such periods in the QSD record, we summed the number of thermal-years within 30-year windows (following the WMO definition of climatic normals) where $\delta^{18}O$ (A_n) values exceed (are <70%) each period's mean. The number of positive deviations within each window was counted to identify periods during which ENSO+ conditions occurred more/less frequently than the multi-decadal average (Figure 4a).

We compared our QSD reconstructed ENSO+ frequency against results from the Paleo Hydrodynamics Data Assimilation model (PHYDA). PHYDA is a global model that assimilates 2978 paleoclimate proxy records with physical ocean-atmosphere constraints to reconstruct hydroclimate and dynamical variables, particularly drought severity, over the past two millennia (Steiger et al., 2018, 2021). PHYDA has been used to infer ENSO activity through teleconnections to global hydroclimate (Steiger et al., 2021). As PHYDA provides seasonal–annual resolution, we extracted modeled El Niño events for the studied period, defined as when the Niño 3.4 SSTs exceed +0.5°C from November to March and summed their interdecadal frequency. We use these results from the PHYDA model to generally validate the QSD reconstruction.

Modeling of ENSO-neutral and ENSO+ agroecological niches

To evaluate how potential agroecological niches may change between ENSO-neutral and ENSO+ conditions, we developed spatial models of viable agricultural areas under different cultivation strategies. Temperature and moisture (PAW) are critical variables affecting plant productivity. We evaluate the extent to which temperature constrained agroecological niches in the study region by calculating growing degree days (GDD), and we evaluate the effects of ENSO+ enhanced PAW on vegetation by measuring trends in gross primary productivity (GPP) using a time series of Sentinel 2A/B multispectral (S2-MSI) imagery (Vining et al., 2022). While temperature and PAW are primary constraints for all vegetation (cultivated and non-cultivated), edaphic and topographic variables (natural or anthropogenic) significantly affect which areas are favored for cultivation. We use these requirements to determine a generic agricultural niche that could have been utilized regardless of cultivation strategies. We further differentiate between areas that most probably were cultivated using irrigation strategies (viable regardless of ENSO status, except for flooding risk) and with dry farming (viable only when available moisture increased, such as during ENSO+ conditions).

Calculation of growing degree days. Plant growth in all regions is constrained by available GDD – periods during which mean temperatures meet plant-specific minimum/maximum temperature requirements. At Chicama's tropical latitude, GDD follow elevational gradients and are not strongly affected by seasonality. Paleoclimate records do not indicate major increases/decreases in mean annual temperature over the past 2 kyr, and modern conditions provide a reasonable approximation of past temperatures. We use temperature requirements for two staple Andean cultivars, corn (*Zea* sp.) and potato (*Solanum* sp.) and SENAMHI temperature records from Casa Grande and San Benito to estimate GDD in the study region using the formula:

$$GDD = Tmax + Tmin \;/\; 2 - Tbase \quad (1)$$

where T_{max} is the daily maximum temperature, T_{min} is the daily low temperature, and T_{base} is the plant-specific minimum temperature development threshold.

Geomorphological constraints on agricultural activity. Elevation, slope, and soil depth are the principal edaphic and topographic factors differentiating cultivable from non-cultivable areas. Archeological and modern irrigation canals (Clément, 2017; Huckleberry et al., 2018; Kus, 1975; Netherly, 1984; Watson, 1979) and "reclamation" of planting surfaces, as well as climate-driven overbank flooding, have left a heavy cumulative imprint on Chicama's deltaic plain. Anthrosols 0.2–1 m thick developed in portions of the Chicama Valley between approximately 1.8 and 0.4 kyr BP (Goodbred et al., 2020; Vining, 2018). In other areas of the deltaic plain, remnant planting surfaces dating from ca. 3.5 to 0.5 kyr BP are preserved, suggesting little change in soil depth (Clément, 2015; Conrad, 1977; Goodbred et al., 2020) and indicating that anthro-pedogenesis was not uniform across the valley. Outside of the deltaic plain, low rates of geomorphological transformation limit the extent to which topographic and edaphic factors have changed dramatically over this study's relatively recent temporal window of interest (the past 1.3 kyr). Other paleo-edaphic variables can be difficult to constrain; soil organic matter (SOM) and plant-available nutrients (PAN) can change over relatively short periods, including being enhanced/depleted by anthropogenic activity (c.f., Goodbred et al., 2020; Vining, 2018). Thus, current soil depth and slope conditions reasonably reflect those of our study period, and we rely on these criteria to delimit a generic model of areas suitable/unsuitable for cultivation.

Elevation and slope values (degrees) were derived from the Advanced Spaceborne Thermal and Emissivity Radiometer global digital elevation model (ASTER GDEM v3). The GDEM was hydrologically-conditioned and resampled to 15 m resolution using bilinear interpolation. Slope values were binarized into suitable/unsuitable for occupation using the $\pm 1\ \sigma$ range of values at a 25% random jackknife sample of known archeological sites.

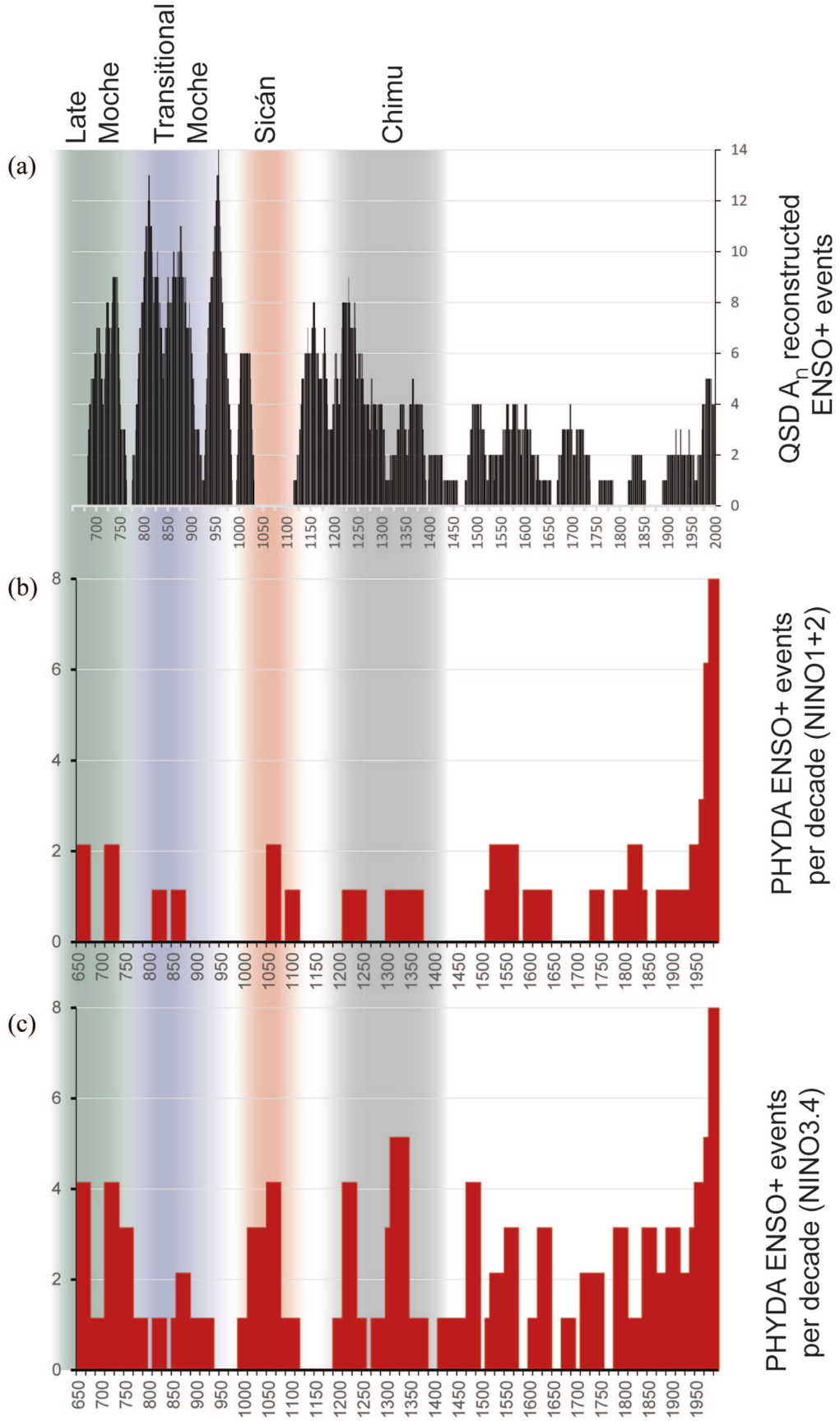

Figure 4. (a) Late-Holocene ENSO+ frequencies reconstructed from the QSD An proxy record. Number of annual events exceeding 30 years normal are shown. (b) PHYDA reconstructed ENSO+ frequencies for the NINO 1+2 region. (c) PHYDA reconstructed ENSO+ frequencies for the NINO 3.4 region. Cultural phases shown in Figure 6 are highlighted.

(This jackknife sample was removed from samples subsequently used to estimate agroecological niches). Edaphic factors were constrained using ISRIC SoilGrids global data. As with topographic factors, we binarized soil variables into suitable/unsuitable for cultivation using minimum (maximum) soil depth criteria of 20 (60) cm, the active root zone for most cultivars. We

combined the soil and slope binary layers into an ordinal ranking of non-agricultural, less-preferred, and most-preferred areas for cultivation. This results in a spatial model of a generic potential agricultural niche (Figure 5a). This model is insensitive to strategies by which water is delivered to plants, and we further refine it into probable irrigation- and dry-farming niches (see below).

Estimation of ENSO-neutral irrigated agricultural niches. Irrigated and dry-farming result in two agro-ecological "niches," which differ based on the methods of delivering moisture to agricultural fields. To delimit the potential irrigation-agriculture niche, we digitized canals recorded by Watson (1979), Netherly (1984), and Clément (2015). All areas downslope from the closest "maximum elevation canal" (Ortloff et al., 1982) we assume could potentially have been cultivated with gravity-fed irrigation from that canal, while areas upslope from the respective maximum elevation canal we assume were inaccessible to it. We used the intersection of the generic agricultural niche and irrigable areas model to define an irrigation-agriculture niche (Figure 5b). Cultivation in this area presumably would have been dependent on irrigation to redirect surface water, with nominal inputs from meteoric precipitation. Thus, this likely represents the major agroecological niche during ENSO-neutral conditions.

Estimation of an expanded agricultural niche during ENSO+ conditions. The generic and irrigated agricultural niche models estimate areas of potential agricultural activity independent of ENSO+ moisture. During the most recent very strong EP ENSO+ (2016–2017), increased PAW from ENSO+ precipitation resulted in arid-adapted vegetation blooms in the deserts surrounding the Chicama Valley. In a companion publication (Vining et al., 2022), we detail the steps used to quantify these effects as trends in GPP; we summarize that analysis below. GPP is the amount of energy photochemically stored by plants per unit area per unit time and is a critical variable for estimating Net Primary Productivity (NPP, the amount of biomass available to consumers). NPP cannot be estimated without plant community-specific parameters, however, and we consequently rely on GPP in our model.

We quantify GPP from a time series of Sentinel 2A and 2B multispectral images (S2-MSI) acquired from the European Space Agency Copernicus Open Access Hub (Copernicus, 2017). Seventeen S2-MSI level 1C scenes spanning the period 02 May 2016–31 July 2018 and having $\leqslant$5% cloud cover were selected. Radiance data were corrected to ground reflectance using scene-specific ephemeris parameters and a mid-latitude arid atmospheric model. We quantify GPP across six distinct vegetation communities that include three communities composed principally of arid-adapted endemic vegetation and three types of cultivated vegetation. The three non-agricultural communities are defined by phytogeographic and topographic criteria in ONERN (1973: 59–68, table 5-E). We gloss the terms used in the original phytogeographic inventory as "littoral," "piedmont," and "matorral" zones, and the criteria used to identify them in our analysis are specified in Vining et al. (2022). The three types of agricultural vegetation are industrial *Saccharum* and *Saccharum/Oryza* monocultures and small polyculture fields (see Vining et al., 2022). This analysis allows us to compare how ENSO-modulated precipitation can affect cultivated and uncultivated vegetation GPP, potentially expanding the dry-farming niche available to premodern agriculture. In particular, we are interested in whether non-agricultural areas can attain levels of productivity under ENSO+ conditions that are comparable to those achieved in vegetation cultivated using different strategies.

Saccharum and *Oryza* monocultures rely on intensive fertigation and flood irrigation techniques and are inappropriate as premodern agriculture analogs. Small-field polyculture provides the most reasonable analog for premodern cultivation. Small polyculture produces levels of GPP ranging between 124.8 and 252.6 $mg\,C\,m^2\,day^{-1}$. From this, we take 191 $mg\,C\,m^2\,day^{-1}$, the interannual mean GPP for modern small-field polyculture, as a conservatively-estimated threshold of agricultural productivity. Two vegetation communities of arid-adapted vegetation achieved sustained levels of GPP during the 2016–2017 ENSO+ phase that exceeded interannual maxima in small-field polyculture. Peak GPP in the piedmont and matorral phytogeographic subregions reached $276.3 \pm 2.8\,mg\,C\,m^2\,day^{-1}$ and $396.9 \pm 5.2\,mg\,C\,m^2\,day^{-1}$, respectively, and were elevated up to 260 days later (Vining et al., 2022). Productivity in uncultivated vegetation clearly does not directly translate to agricultural potentials. However, this analysis indicates that high levels of productivity are potential in certain desert areas under ENSO+ conditions and further allows us to identify an average level of GPP in certain types of cultivation as a threshold for agricultural viability in other regions. Ultimately, our agroecological niche model examines productive potentials on a cell-wise basis determined by sustained levels of GPP and topographic/edaphic characteristics, irrespective of the phytogeographic region in which it lies.

We binarized our GPP measurements at the mean polyculture threshold to identify areas at each time step in our series that could achieve levels of GPP consistent with agricultural needs. Each binarized mask was factored by the number of days between observations and summed, to estimate the total number of days during which GPP remained above/below this threshold. We relate this result to the GDD requirements of probable cultivars by compiling a list of modern and prehistoric cultivars found in the Chicama Valley from Gálvez Mora and Runcio (2011) and Caramanica (2018) and using the average GDD to maturity for modern analogs from the Iowa State University Agricultural Extension and Outreach to determine which areas within the Chicama Valley might have been viable for each cultivar. Minimally $\geqslant$45 days above the minimum productivity threshold are necessary for the fastest maturing cultivars, with common Andean cultivars typically requiring 90–120 days. GPP data were ordinally ranked according to these intervals to produce a dataset showing locations that could sustain levels of GPP $\geqslant$ mean small field polyculture for periods sufficient for each cultivar to reach maturity.

The intersection of this model with the generic agroecological niche identifies areas in Chicama that can reach minimum productivity thresholds during ENSO+ conditions and meets other agroecological niche criteria. This defines the possible dry-farming niche under generalized ENSO+ conditions (Figure 5c). While there are limitations to these assumptions, this allows us to estimate which areas of the valley potentially could have supported analogous cultivars throughout growth to maturation, if cultivation in these areas relied only on ENSO-derived moisture.

Reconstructing agroecology usage in archeological periods

To examine how past populations may have responded to or capitalized on ecological changes driven by paleo-ENSO activity, we compare temporally-binned archeological settlement data to agricultural niche models. Prior archeological survey data (Elera Arévalo, 1998; Bird and Hyslop, 1985; Caramanica, 2018; Chauchat, 1975; Chauchat et al., 1998; Clément, 2015; Conrad, 1977; Gálvez Mora and Briceño, 2001; Krzanowski, 1985; Leonard and Glenn, 1992; Netherly, 1984; Shoji, 2018; Toshihara, 2002; Vining, 2018) were integrated into a single database. Different cultural classifications were reconciled using a look-up table (LUT) approach, where each phase was assigned a start/end date. This LUT allows us to reconcile divergent categorical schema with a common absolute chronology, which could be related to the timing of paleoclimatic events (see supplemental materials). Only archeological loci with at least one identified archeological period and where there was evidence for occupation and/or agricultural activities were incorporated into our analysis. Settlement distributions were subsequently parsed using 200-year bins to relate them to

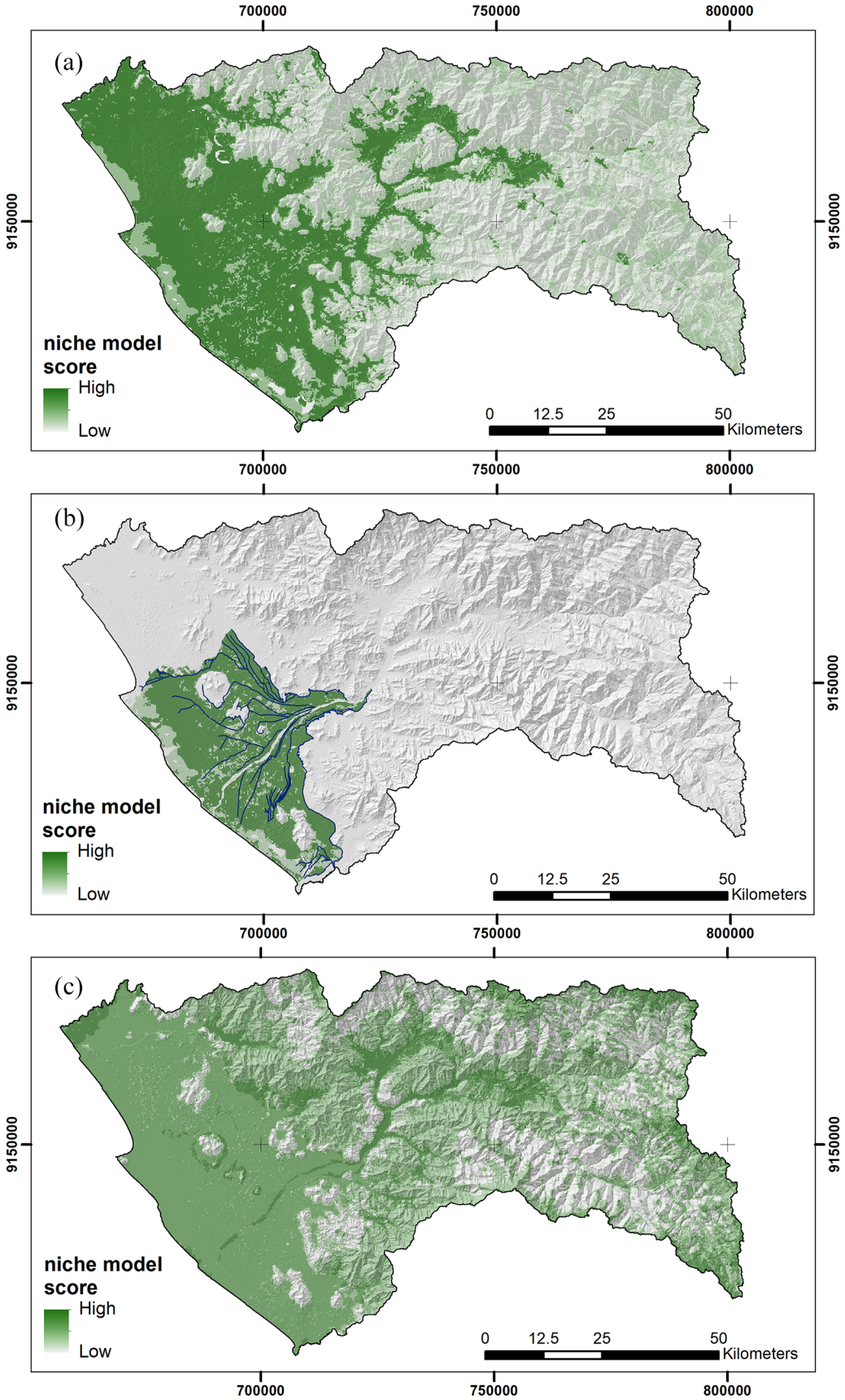

Figure 5. Agricultural niches available in the Chicama Valley based on topographic and edaphic criteria and mechanism of water-availability. (a) the generic agroecological niche derived from edaphic and topographic factors. (b) the area cultivable by extant and archeological irrigation canal systems (largely conforming to the floodplain). (c) The expanded agricultural niche that could be utilized by dry-farming and/or localized irrigation networks that redirect surface/groundwater from meteoric sources.

ENSO reconstructions. Settlement patterns for three periods between 1270 and 500 BP, corresponding to the period of overlap with the QSD record up to the Chimu Period are shown in Figure 6.

Diachronic settlement patterns are compared to the agroecological niche models using maximum entropy (MaxEnt) niche estimation methods. MaxEnt, originally developed for species

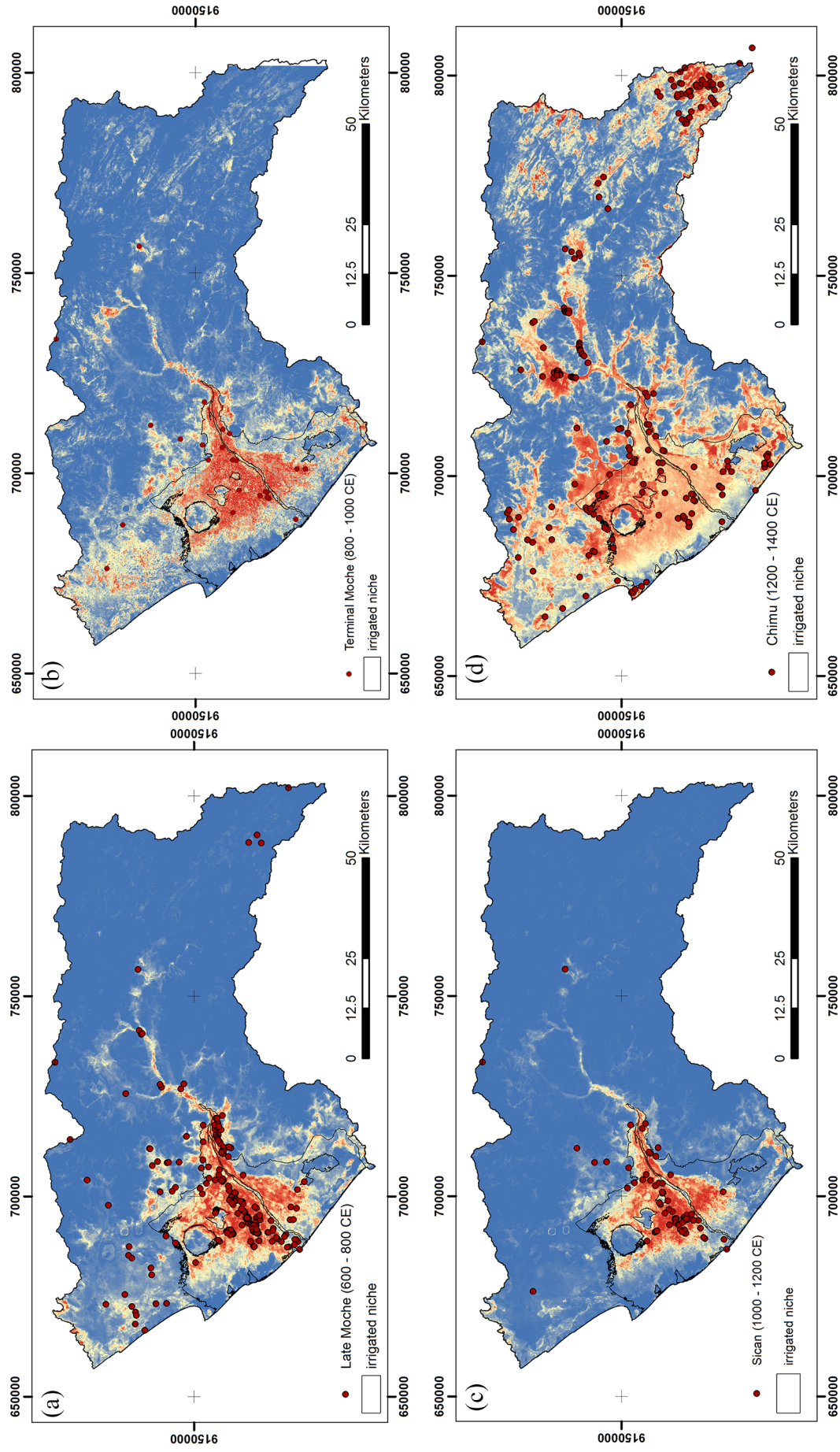

Figure 6. Maximum Entropy niche models and distribution of archeological settlements and agricultural features for three cultural periods during the late-Holocene, 1350–550 BP. (a) Late Moche Period. (b) Transitional Moche Period. (c) Sicán Period. (d) Chimu Period.

Table 1. 2016–2017 ENSO+ precipitation totals at San Benito relative to monthly mean (1964–2020).

	Nov	Dec	Jan	Feb	Mar	Apr	May	Jun
Monthly average precipitation	7.6	19.6	59.6	110.0	155.0	49.4	9.4	2.2
2016–2017 monthly total precipitation	0.0	11.6	99.2	496.5	945.4	45.6	12.0	0.0
2016–2017 percent of average	34.1	59.0	166.5	451.2	610.0	92.3	127.6	0.0

Table 2. Pearsons ρ correlation coefficients for DJF NINO 1 - 4 SSTA, DJF - MAM precipitation at San Benito, and Quelccaya Summit Dome thermal year δ18O.

	NINO1+2	NINO3	NINO3.4	NINO4
San Benito	0.72	0.43	0.26	0.04
QSD $\delta^{18}O$	0.14	0.33	0.41	0.6

ecological niche distribution modeling, provides a highly effective approach for estimating the strength of relationships between environmental factors and archeological locations (McMichael et al., 2014; Vining and Burns, 2018; Yaworsky et al., 2020). The most problematic assumption in archeological modeling is that pseudoabsences due to sampling/preservation biases indicate true absences. MaxEnt niche estimation accommodates presence-only data and estimates niches based on the most uniform probability distribution of environmental variables coinciding with presence-only data (Phillips et al., 2006).

Results and discussion

Estimation of paleo-hydroclimatic conditions in Chicama

Pluviometric data show greatly enhanced rainfall at San Benito during the 2016–2017 ENSO+ period (Table 1). Monthly rainfall totals during the ENSO+ wet season (DJF–MAM) were as much as 610% of mean monthly accumulation. Importantly, individual ENSO+ phases do not consistently result in the same local precipitation patterns (Bendix, 2000; Goldberg et al., 1987; Lagos et al., 2008; Tapley and Waylen, 1990). However, given the moderate–strong relationships (at 99% confidence level) between SSTA and study region multi-decadal precipitation, it is probable that these multidecadal periods of ENSO+ conditions resulted in enhanced direct precipitation on the Chicama coastal desert.

Pairwise Pearson's ρ coefficients for San Benito precipitation, QSD $\delta^{18}O$ and thermal year (July–June) SSTA in the NINO 1–4 regions are shown in Table 2 (see Figure 2). These variables range from moderately to strongly correlated. Nonetheless, correlations between rainfall data, NINO 1–4 SSTA, and QSD ENSO proxies allow us to estimate approximate hydroclimatic conditions in Chicama over the past ~1300 years, including inferring periods during which ENSO+ conditions occurred with greater/lesser frequency.

Precipitation anomalies at San Benito are very strongly correlated ($r=0.72$, $p<0.01$) with SSTA in the NINO1.2 region, while correlations weaken toward the central Pacific. Conversely, QSD $\delta^{18}O$ is most strongly correlated with central Pacific SSTA ($r=0.6$, $p<0.01$) and weakens toward the EP (Thompson et al., 2011, 2013). This indicates that more proximate Eastern Pacific dynamics have a stronger effect on precipitation in the Chicama study region, while precipitation at QSD is effected more strongly through central Pacific teleconnections. Isotopic models further support this relationship (Vuille and Werner, 2005). These relationships are modulated by ITCZ migration, the influence of Pacific SST on Atlantic-Amazonian source moisture, and recent (modern) anthropogenic effects (Bradley et al., 2003; Thompson et al., 2013; Vuille et al., 2003). Due to this variability, relationships between single pairs of records are moderately correlated at best, while correlations between composite sequences are stronger.

Similar levels of correlation between San Benito precipitation, QSD $\delta^{18}O$, and NINO SSTA are found near the boundary between the Eastern and Central Pacific. San Benito precipitation and QSD $\delta^{18}O$ are correlated with NINO 3 region at $r=0.41$ and $r=0.33$, respectively (both $\rho<0.01$). We use the similar levels of correlation in the NINO 3 region to infer that QSD provides a minimal reconstruction of CP ENSO activity affecting the EP/north coastal Peru region, while underrepresenting EP ENSO events.

Despite sensitivities to different NINO SSTA, QSD A_n and $\delta^{18}O$ can be used to infer the frequency of CP and EP ENSO events that may have influenced San Benito hydroclimatic conditions. Reconstructions based on QSD A_n and $\delta^{18}O$ likely capture strong ENSO+ phases that develop within the central Pacific and adjacent regions. Weaker ENSO+ conditions and/or events that developed only in one NINO region, such as the 2016–2017 EP ENSO+, are underestimated in QSD proxies. Consequently, this model of paleo-ENSO activity is not sufficient to identify discrete events affecting Chicama, but can be used to identify decadal-scale frequencies of intensified ENSO activity. PHYDA modeling results provide additional support for decadal changes in the intensity of ENSO activity.

The frequency of ENSO-like conditions within 30-year normals varies considerably over the length of the QSD record, from approximately AD 650 to 2000 (Figure 4a). The QSD record indicates multi-decadal periods of enhanced ENSO+ conditions from approximately AD 700–750, 800–900, 950–975, 1125–1260, and recently after 1950. The QSD record further indicates decreased ENSO activity during the LIA, from approximately AD 1450 to 1920. Paleo-ENSO reconstructions from Laguna Pallcacocha (Moy et al., 2002) and Chilibrillo Cave (Lachniet et al., 2004) also broadly agree with this pattern of increased/decreased EP ENSO activity over the last 1.3 kyr BP.

Paleo-ENSO activity reconstructed from the PHYDA model (Figure 4b and c) agrees with broad trends in the QSD paleo-ENSO frequency reconstruction, though there are important discrepancies. PHYDA indicates higher frequencies of ENSO+ conditions in NINO 1+2 and 3.4 in the decades prior to ca. 875 CE and after approximately 1200 CE. PHYDA suggests the period 900–1200 CE is characterized by generally infrequent ENSO+ conditions, but is abruptly interrupted by two episodes of greatly increased ENSO+ frequency approximately 1050–1080 (NINO 1+2, Figure 4b) CE or 1030–1060 CE (NINO 3.4, Figure 4c). The QSD reconstruction, importantly, does not show this interlude. The discrepancy may be due to the influence of other inputs on the PHYDA global model.

Expanded agroecological niches during ENSO+ phases

Enhanced meteoric precipitation during ENSO+ periods serves to expand moisture availability in non-irrigated regions of the desert, in the forms of direct meteoric water, groundwater recharge, and localized surface flow. As temperature has little constraining influence on agricultural potentials, the net effect of enhanced moisture is the dramatic expansion of productive niches in parts of the valley that, during most years, are hyper-arid and

largely barren. Our baseline for this model is the generic agricultural niche determined by edaphic and topographic characteristics, which we differentiate into viable irrigable and dry-farming niches based on the presence of canals (in case of the former) or GPP productivity thresholds with ENSO precipitation (in the case of the latter). The expansion of productive niches observed during the 2016–2017 EP ENSO+ phase provides a means to estimate how cultivable area in Chicama could have expanded during past ENSO+ periods, even as normally cultivated floodplains underwent flooding; irrigation infrastructure may have been damaged by flooding and landslides on saturated slopes; and production demands likely intensified as other food sources and economic activities were disrupted by these same ENSO+ conditions.

We estimated GDD for *Zea* sp. and *Solanum* sp. following equation (1) (see Supplemental Material). Both cultivars were important as staple foods and for financing political economies during the prehispanic period. GDD permit cultivation of *Zea* sp. throughout the austral wet season (roughly late October through late May). Temperature may have limited *Zea* sp. cultivation if seasonal GDD did not coincide with moisture availability, particularly at the elevation of San Benito. Available GDD permit cultivation of *Solanum* sp. year-round in both locations and was not a limiting factor for tubers.

As we have limited ability to reconstruct PAW during paleoclimatic phases, we rely on 2016–2017 ENSO+ vegetation dynamics as a proxy measure from which we infer the effects of past enhanced ENSO+ moisture on PAW and the expansion of agriculturally-viable regions. The GPP time series shows a dramatic but geomorphologically-contingent response of vegetation communities to ENSO-derived precipitation during the 2016–2017 El Niño (detailed in Vining et al., 2022). GPP increased in all phytogeographic subregions (except the coastal littoral) with 2016-2017 ENSO+ conditions. GPP in agricultural areas increases by 11–90% over peak ENSO-neutral values, despite damages to infrastructure from avulsion, flooding, and slope failures.

Desert vegetation responses to ENSO-derived moisture are dramatic. During ENSO neutral years, desert vegetation is minimal and GPP in the three uncultivated phytogeographic subregions we examined is well below mean GPP in cultivated areas. ENSO+ GPP in the desert piedmont and matorral regions peaks at 276 ± 0.03 and 397 ± 0.05 mg C/m^{-2} day^{-1}, respectively, a more than 260% increase over peak productivity during ENSO neutral years. Notably, peak GPP in desert phytogeographic subregions is commensurate with GPP in intensively-cultivated areas. Levels of arid-land GPP that are greater than dry season/ENSO-neutral conditions are recorded as late as 14 October 2017, 6 months following peak ENSO rainfall.

We take GPP = 191 mg C/m^{-2} day^{-1}, the mean interannual value in modern polyculture fields, as the minimum threshold for small-scale agricultural viability. With the exception of the coastal littoral, inland piedmont and matorral subregions sustained sufficiently high and sustained levels of GPP during the 2016–2017 ENSO+ to allow cultivation of most Andean crops that require between 45 and >240 days to maturation. The intersection of the ENSO+ plant-productive niche with the generic agricultural niche indicates an expanded potential agroecological niche (Figure 5c). Most of the expanded area lies inland and upland, away from the irrigable niche. These results indicate that vegetation productivity can increase dramatically in desert areas with enhanced ENSO+ rainfall and can match or even exceed levels of productivity achieved in conventional agriculture.

These results, based on a single ENSO+ event in 2016–2017, are consistent with prior studies documenting sustained and often positive effects of earlier ENSO+ precipitation on communities of arid-adapted endemic vegetation (Albán et al., 2006; Cano et al., 1999; Dillon and Rundel, 1990; Erdmann et al., 2008; Richter, 2005; Rodríguez et al., 2005; Tovar et al., 2018). Endemic vegetation responses to ENSO conditions do not necessarily translate to domesticated cultivars. However, PAW increased sufficiently during the 1982–1983 and 1997–1998 ENSO+ events that corn (*Zea* sp.) and wheat, requiring up to 190 GDD to maturation, were cultivated within desert areas, "indicating the presence of enough available moisture for agriculture" (Dillon and Rundel, 1990: 497; Gálvez Mora and Runcio, 2011). Positive effects from a single ENSO+ period were recorded in arid-adapted herbaceous vegetation up to 7 months later (Vining et al., 2022) and up to 3–6 years later in dry forest communities (Richter, 2005). Decadal-scale periods during which "ENSO-like" conditions were more prevalent likely would have similar sustained and overlapping effects on the region's ecological functioning, including providing benefits to secondary and tertiary consumers.

Sensitivity of archeological settlement to ENSO patterns

A database of >1200 published archeological loci data allows us to reconstruct settlement patterns through broad cultural phases, despite limitations due to chronological precision. We evaluate potential responses to increased multidecadal ENSO+ frequency during three major cultural periods (late Moche, Sican, and Chimu) which overlap with QSD A_n and $\delta^{18}O$ records from AD 650 to 1530.

Archeological settlement occurs within the irrigable and expanded agricultural niches and changes diachronically across these subregions (Figure 6). Maximum entropy models (Figure 6a and b) show human settlement between ca. AD 600 and 1000 (Late Moche and Transitional Moche periods, $n = 251$) was approximately evenly distributed between the irrigable floodplain (56% of sites) and the desert interior (43.8% of sites). Both QSD A_n and PHYDA reconstructed ENSO activity indicate generally increased ENSO+ frequency during this period (Figure 4). The specific dynamics differ, however. During the subsequent Sicán period (ca. 1000–1200 AD, $n = 84$), settlement is concentrated within the floodplain (81% of sites) with fewer sites recorded in the desert interior (19%, Figure 6c). In both QSD and PHYDA models, this cultural period overlaps with a general decrease in ENSO+ activity, except for the interlude of abruptly increased ENSO+ activity indicated by the PHYDA models (see above). The Chimu period (ca. 1200–1470 AD, $n = 242$) sees the greatest dispersal of sites with proportionally fewer in the irrigable plain (37.6%) and many more in the desert interior and uplands (62.4%) where agriculture aided by well-developed agricultural technology appears to have capitalized on changing ecological conditions (Clément, 2015, 2017). This dispersal overlaps with an increase in ENSO+ frequency in the QSD and PHYDA reconstructions starting ca. 1130–1200 CE and continuing as late as ca. 1375 CE. Chi-square values ($\chi^2 = 158.75$, df = 7, p-value < 2.2e−16) show that the different distributions of settlement across irrigable and rain-fed agroecological niches in the different periods is highly significant (Table 3).

Generally, archeological patterns track with changes in ENSO+ frequency. The exception to this is the lack of Sicán settlement in desert regions during an interlude of reinvigorated ENSO+ activity indicated by the PHYDA model in the mid–late 11th century CE (Figure 4). The shifts between these extremes of may have created scenarios of risk during the Sicán period (centered in the Chicama Valley on 1020–1175 CE, Santana-Sagredo et al., 2020). Conversely, overall increased ENSO+ frequencies, without alternating between extremes, in the centuries before 900 and after 1200 CE may have resulted in sustained hydroclimatic phase shifts and less socio-ecological disruption. As an alternate explanation, there may have been little socio-ecological impetus during the Sicán period to capitalize on potential ENSO-driven ecological changes. ENSO+ events create ecological conditions

Table 3. Pearson's Chi-squared test of the distribution of sites per cultural phase across likely agricultural niches.

Observed values				Percentages			Expected values		row proportions	
	Irrigable area	Arid area	Total	Irrigable area	Arid area	Total	Irrigable area	Arid area	Irrigable area	Arid area
Guañape	9	128	137	6.6	93.4	100	57	80	0.066	0.934
Cupisnique	9	40	49	18.4	81.6	100	20	29	0.184	0.816
Gallinazo	87	111	198	43.9	56.1	100	83	115	0.439	0.561
Salinar	87	111	198	43.9	56.1	100	83	115	0.439	0.561
Moche	141	110	251	56.2	43.8	100	105	146	0.562	0.438
Sican	68	16	84	81.0	19.0	100	35	49	0.81	0.19
Chimu	91	151	242	37.6	62.4	100	101	141	0.376	0.624
Inka	95	151	246	38.6	61.4	100	103	143	0.386	0.614

X-squared = 158.75, df = 7, p-value < 2.2e−16.

that could be taken advantage of, but might not have been. This discrepancy highlights the likely significance of contingent socio-ecological decision-making with changing hydroclimates.

Coupled hydroclimate-agroecology models indicate that marginal arid regions can transform to productive niches during ENSO+ events. ENSO-enabled dry farming could support short season cultivars as well as cultivars requiring growing seasons of >200 days. The sustained effects of increased PAW from meteoric sources are critical; enhanced GPP persists well after the direct effects of ENSO+ weather events themselves due to increased soil moisture, surface flow, and shallow groundwater recharge. Potential agriculturally-productive niches expanded dramatically in the growing periods following ENSO-positive conditions. We hypothesize that this productivity could partially offset losses (including to irrigation-dependent agriculture) during the same ENSO events.

Conclusion

Previous archeological investigations on the arid Andean coast have emphasized ties between cultural development, agroecological productivity, and water risk, with el Niño events occupying a central role in this discussion (e.g. Billman and Huckleberry, 2008; Dillehay and Kolata, 2004; Moseley et al., 2008; Nesbitt, 2016; Sandweiss and Quilter, 2008; Sandweiss et al., 2007; Shimada et al., 1991). ENSO events are typically framed as profoundly adverse "catastrophes," – stochastic environmental risks that inhabitants struggled to survive. There is less discussion of adapting to or even planning for this periodic climatic change. We see this characterization as incomplete and have integrated multiple lines of evidence to better understand the spatio-temporal domains of ENSO-driven risk as well as the variability of past human responses.

Here, we've compared patterns in human settlement to the modeled expansion and contraction of productive zones in the Chicama Valley during ENSO+/pluvial conditions. These models leverage ENSO SSTA, meteorological, paleoclimatic, geospatial, and archeological evidence to better understand the net ecological transformations that occur during ENSO+ periods, including risks and opportunities. We find that multidecadal periods of increased ENSO+ activity in the late-Holocene likely increased effective moisture in Chicama, which in turn also enhanced PAW and GPP in areas that currently are hyperarid deserts. During recent ENSO+ periods, potentially agriculturally-productive niches expanded dramatically; climatic data support that this mechanism would function similarly under paleo-hydroclimate scenarios. Archeological settlement patterns support the hypotheses that agricultural communities at least occasionally capitalized on expanded productive niches linked to ENSO+ periods. Expanded productive niches during ENSO+ periods could offset, at least partially, losses to built environments (including irrigation-dependent agriculture) during the same and subsequent ENSO events.

The correspondence between past periods of strengthened ENSO activity and archeological settlement in currently arid desert regions accords with recent work linking ENSO activity with dry- and groundwater-fed desert cultivation (Caramanica et al., 2020; Gálvez Mora and Runcio, 2011). These localized fields and irrigation systems, once developed, could readily be rehabilitated and prepared for cultivation during subsequent el Niños. Individuals could buffer anticipated ENSO risk by mobilizing adaptive economic activities either in anticipation of ENSO+ conditions or in response to them (Gálvez Mora and Runcio, 2011).

These results suggest prehispanic communities in Chicama used a complicated risk calculus. These communities employed multiple agroecological strategies during periods of strengthened ENSO activity, presumably to mitigate risks resulting from the intersection of abrupt climatic changes and the socio-technological dependencies. Our results further suggest an awareness of the ecological changes – both risks and opportunities – posed by abrupt but episodic ENSO climate changes. The uneven distribution of productive niches during ENSO+ phases likely distributed risk and opportunity differentially across the regions' inhabitants, which itself may have created additional structural challenges or opportunities. This response highlights that "risk societies" are frequently aware of a risk's various dimensions, voluntarily assume aspects of risk, but have developed strategies that shift anticipated risks across their social segments.

Critical issues that remain to be evaluated are the extent to which premodern Andean communities had an awareness and knowledge of ENSO dynamics, including their ecological effects, and the extent to which organizational and technological changes may have emerged as risk-responses. Increasing frequencies of ENSO events on generational – intergenerational time scales plausibly could lead to emergent ecological knowledge bases, which in turn would enable forecasting and preparing for ENSO events. Imagery on Moche artifacts suggests that their knowledge of ENSO ecological effects was comprehensive, fine grained, and included observations of interspecific behavioral changes during ENSO+ events (Bourget, 2016: 198–291). Ethnohistorically, ecological knowledge was sufficiently sensitive to forecast coming ENSO+ phases based on observation of atmospheric and marine conditions (Orlove et al., 2000; Schaedel, 1988: 31). Knowledge of and an ability to forecast ENSO+ becomes even more critical, and arguably more likely, during periods when ENSO events occurred with more frequency.

Several climatic models predict future increases in the frequency and intensity of ENSO events due to anthropogenic oceanic and atmospheric warming (Cai et al., 2020; Timmermann et al., 1999; Trenberth and Hoar, 1997; Wang et al., 2019; Yeh et al., 2009). This potentially will result in dramatic changes to the arid environments of western South America. In light of these

forecast changes, the sensitivity of local cultivation patterns to global and regional climate change (e.g. Ramankutty et al., 2002) is an important element of climate risk the region faces. Linked paleoclimate and archeological data have the potential to add specificity to generalized forecasts of climate change impacts. Paleoclimate data can identify periods of heightened ENSO frequency/strength that are analogs for future conditions. Archeological remains are highly visible on Peru's arid coast, and, while imperfect as paleoclimatic proxies, can be used to reconstruct human responses as "end-users" of hydroclimatic conditions (Vining et al., 2019, 2022). This integrative approach can better inform our understanding of climate-driven risk in arid and hyperarid regions.

Acknowledgements

We thank Dave Stahle for his suggestions related to the climatic analysis.

Data availability

Sentinel 2A and 2B data were accessed through the ESA's Copernicus Data Open Access Hub and through the USGS Land Processes Distributed Active Archive Center (LP DAAC).

Funding

The author(s) disclosed receipt of the following financial support for the research, authorship, and/or publication of this article: Portions of this research were supported by a National Science Foundation grant (BCS-1848699) to PI Vining and co-PIs Hillman and Contreras. E. Tejedor was partially supported by NSF-PIRE (OISE-1743738).

ORCID iDs

Benjamin R Vining https://orcid.org/0000-0001-9375-5151
Daniel A Contreras https://orcid.org/0000-0002-8127-8789

Supplemental material

Supplemental material for this article is available online.

References

Abbott MB, Wolfe BB, Wolfe AP et al. (2003) Holocene paleohydrology and glacial history of the central Andes using multiproxy lake sediment studies. *Palaeogeography Palaeoclimatology Palaeoecology* 194: 123–138.

Albán L, Matorel M, Trías J et al. (2006) Reforestación extensiva con algarrobo (Prosopis pallida) en la región desértica de Piura, Perú. *Zonas áridas* 7(1): 244–252.

Anderson C (2020) senamhiR: A collection of functions to obtain Peruvian climate data. Available at: https://gitlab.com/ConorIA/senamhiR/ (accessed 18 March 2021).

Andrus CFT, Crowe DE and Romanek CS (2002) Oxygen isotope record of the 1997-1998 El Niño in Peruvian sea catfish (*Galeichthys(Galeichthys peruvianus*) otoliths. *Paleoceanography* 17(4): 5–1.

Andrus CFT, Sandweiss DH and Reitz EJ (2008) Climate change and archaeology: The holocene history of El Niño on the coast of Peru. In: Reitz EJ, Scudder SJ and Scarry CM (eds) *Case Studies in Environmental Archaeology*. New York, NY: Springer, pp.143–157.

Ashok K, Behera SK, Rao SA et al. (2007) El Niño Modoki and its possible teleconnection. *Journal of Geophysical Research: Oceans* 112: C11.

Beck U and Wynne B (1992) *Risk Society: Towards a New Modernity*. London: SAGE.

Bendix J (2000) Precipitation dynamics in Ecuador and northern Peru during the 1991/92 El Nino: A remote sensing perspective. *International Journal of Remote Sensing* 21(3): 533–548.

Billman BR (2002) Irrigation and the origins of the southern Moche state on the north coast of Peru. *Latin American Antiquity* 13(4): 371–400.

Billman BR and Huckleberry G (2008) *Deciphering the Politics of Prehistoric El Niño Events on the North Coast of Peru.* In: Sandwiess D and Quilter J (eds) El Niño, Catastrophism, and Culture Change in Ancient America. Washington, DC: Dumbarton Oaks Research Library and Collection, Harvard University Press, pp.101–128.

Bird BW, Abbott MB, Rodbell DT et al. (2011) Holocene tropical South American hydroclimate revealed from a decadally resolved lake sediment δ18O record. *Earth and Planetary Science Letters* 310(3-4): 192–202.

Bird JB and Hyslop J (1985) The preceramic excavation at the Huaca Prieta Chicama Valley, Peru. *Anthropological papers of the American museum of natural history* 62(1): 8–294.

Bourget S (2016) *Sacrifice, Violence, and Ideology Among the Moche: The Rise of Social Complexity in Ancient Peru*. Austin, TX: University of Texas Press.

Bradley RS, Vuille M, Hardy D et al. (2003) Low latitude ice cores record Pacific sea surface temperatures. *Geophysical Research Letters* 30(4): 1–4.

Briceño J (1999) Quebrada Santa María: Las puntas en cola de pescado y la antigüedad del hombre en Sudamérica. *Boletín de Arqueología PUCP* 3: 19–39.

Briceño J (2011) Últimos descubrimientos del paijanense en la parte alta de los valles de Chicama, Moche y Vir norte del peP-erúNuNuevaserspectivas obre los primeros cazadores-recolectores n losanAndesedeuSudaméricaicundefined. *Boletín de Arqueología PUCP* 15: 165–203.

Cai W, McPhaden MJ, Grimm AM et al. (2020) Climate impacts of the El Niño–Southern Oscillation on South America. *Nature Reviews Earth & Environment* 1(4): 215–231.

Cano AC, Roque J, Arakaki M et al. (1999) Diversidad floristica de las Lomas de Lachay (Lima) durante el evento El Niño 1997-98. *Revista Peruana de Biologia* 6(3): 125–132.

Caramanica A (2018) *Land, labor, and water of the ancient agricultural Pampa de Mocan, North Coast, Peru*. Dissertation, Harvard University, Cambridge, MA.

Caramanica A, Huaman Mesia L, Morales CR et al. (2020) El Niño resilience farming on the north coast of Peru. *Proceedings of the National Academy of Sciences* 117(39): 24127–24137.

Chattopadhyay R, Dixit SA and Goswami BN (2019) A modal rendition of ENSO diversity. *Scientific Reports* 9(1): 1–11.

Chauchat C (1975) The Paijan complex, Pampa de Cupisnique, Peru. *Nawpa Pacha: Journal of Andean Archaeology* 13: 85–96.

Chauchat C, Gálvez C, Briceño J et al. (1998) *Sitios arqueológicos de la zona de Cupisnique y margen derecha del valle de Chicama*. Instituto Nacional de Cultura La Libertad.

Clément C (2015) *Paysage socioculturel et architecture dans la culture Chimú: l'implantation humaine à l'intermédiaire recent (1000-1470 apr. J.-C.) dans la vallée de Chicama (côte nord du Pérou)*. Oxford: BAR International Series/Archaeopress.

Clément C (2017) The oasis of the Chicama Valley: Water management from the Chimú to the Spaniards (eleventh to seventeenth century AD) on the north coast of Peru. In: Lavie E and Marshall A (eds) *Oases and Globalization*. Cham: Springer, pp.73–88.

Cobb KM, Westphal N, Sayani HR et al. (2013) Highly variable El Niño-Southern Oscillation throughout the Holocene. *Science* 339(6115): 67–70.

Conrad GW (1977) Chiquitoy Viejo: An Inca administrative center in the Chicama Valley, Peru. *Journal of Field Archaeology* 4(1): 1–18.

Copernicus, (2017) *Sentinel 2A MultiSpectral Instrument Level 1C Data*. European Space Agency retrieved from Copernicus Open Access Hub.

Crate SA (2011) Climate and culture: Anthropology in the era of contemporary climate change. *Annual Review of Anthropology* 40(1): 175–194.

Crate SA and Nuttall M (eds) (2016) *Anthropology and climate change: From encounters to actions*. New York, NY: Routledge.

Dillehay TD, Bonavia D, Goodbred S et al. (2012) Chronology, mound-building and environment at Huaca Prieta, coastal Peru, from 13 700 to 4000 years ago. *Antiquity* 86(331): 48–70.

Dillehay TD and Kolata AL (2004) Long-term human response to uncertain environmental conditions in the Andes. *Proceedings of the National Academy of Sciences* 101(12): 4325–4330.

Dillon MO and Rundel PW (1990) The botanical response of the Atacama and Peruvian Desert floras to the 1982-83 El Niño event. *Elsevier Oceanography Series* 52: 487–504.

Eichler TP and Londoño AC (2013) ENSO impacts on lomas formation in South Coastal Peru: Implications for the pliocene? *Advances in Meteorology* 2013: 1–7.

Ekberg M (2007) The parameters of the risk society: A review and exploration. *Current Sociology* 55(3): 343–366.

Elera Arévalo CG (1998) *The Puémape site and the Cupisnique culture: A case study on the origins and development of complex society in the Central Andes, Perú*. Unpublished doctoral dissertation thesis, University of Calgary, Calgary.

Erdmann W, Schulz N, Richter M et al. (2008) Efectos del fenómeno del Nino 1997–1998 en la vegetación del desierto de Sechura, Región Paita hasta el año 2008. *Arnaldoa* 15(1): 63–86.

Ferreyra R (1993) Registros de la vegetación en la costa peruana en relación con el fenómeno El Niño. *Bulletin de l'Institut français d'études andines* 22(1): 259–266.

Franco R, Gálvez Mora C and Vásquez S (2001) La huaca Cao Viejo en el complejo El Brujo: Una contribución al estudio de los mochicas en el valle de Chicama. *Arqueologicas* 25: 55–59.

Gálvez Mora C and Runcio MA (2011) Eventos ENOS (El Niño, La Oscilación del Sur) y el cultivo de maíz en el desierto del sector medio del valle de Chicama, Perú. *Archaeobios* 5(1): 147–150.

Gálvez Mora C and Runcio MA (2015) Ocupación, movilidad y subsistencia en el desierto de la margen derecha del valle de Chicama, Costa Norte del Perú. *Archaeobios* 9(1): 246–268.

Gálvez Mora C and Briceño J (2001) The Moche in the Chicama Valley. In: Pillsbury J (ed.) *Moche Art and Archaeology in Ancient Peru*. Washington, DC: National Gallery of Art, pp.140–157.

Garcia-Herrera R, Barriopedro D, Hernández E et al. (2008) A chronology of El Niño events from primary documentary sources in northern Peru. *Journal of Climate* 21(9): 1948–1962.

Garnica L (1997) Evaluación ambiental del fenómeno "El Niño 1997-98" en el sector agrario. *Revista Peruana de Biologia* 6(3): 180–182.

Garreaud RD (2009) The Andes climate and weather. *Advances in Geosciences* 22: 3–11.

Gergis JL and Fowler AM (2009) A history of ENSO events since AD 1525: Implications for future climate change. *Climatic Change* 92(3–4): 343–387.

Giddens A (1999) Risk and responsibility. *Modern Law Review* 62(1): 1–10.

Goldberg RA, Tisnado M G and Scofield RA (1987) Characteristics of extreme rainfall events in northwestern Peru during the 1982–1983 El Niño period. *Journal of Geophysical Research: Oceans* 92(C13): 14225–14241.

Goodbred SL, Dillehay TD, Galvéz Mora C et al. (2020) Transformation of maritime desert to an agricultural center: Holocene environmental change and landscape engineering in Chicama River valley, northern Peru coast. *Quaternary Science Reviews* 227: 106046.

Harvell CD, Mitchell CE, Ward JR et al. (2002) Climate warming and disease risks for terrestrial and marine biota. *Science* 296(5576): 2158–2162.

Huckleberry G, Caramanica A and Quilter J (2018) Dating the ascope canal system: Competition for water during the late Intermediate Period in the Chicama Valley, North Coast of Peru. *Journal of Field Archaeology* 43(1): 17–30.

Hudson MJ, Aoyama M, Hoover KC et al. (2012) Prospects and challenges for an archaeology of global climate change. *Wiley Interdisciplinary Reviews: Climate Change* 3(4): 313–328.

Hurley JV, Vuille M and Hardy DR (2019) On the interpretation of the ENSO signal embedded in the stable isotopic composition of Quelccaya Ice Cap, Peru. *Journal of Geophysical Research Atmospheres* 124: 131–145.

Hu Z-Z, Huang B, Zhu J et al. (2019) On the variety of coastal El Niño events. *Climate Dynamics* 52(12): 7537–7552.

Kanner LC, Burns SJ, Cheng H et al. (2013) High-resolution variability of the South American summer monsoon over the last seven millennia: Insights from a speleothem record from the central Peruvian Andes. *Quaternary Science Reviews* 75: 1–10.

Kluger LC, Kochalski S, Aguirre-Velarde A et al. (2019) Coping with abrupt environmental change: The impact of the coastal El Niño 2017 on artisanal fisheries and mariculture in North Peru. *ICES Journal of Marine Science* 76(4): 1122–1130.

Knüsel S, Brütsch S, Henderson KA et al. (2005) ENSO signals of the twentieth century in an ice core from Nevado Illimani, Bolivia. *Journal of Geophysical Research* 110: D01102.

Koons ML (2015) Moche sociopolitical dynamics and the role of Licapa II, Chicama Valley, Peru. *Latin American Antiquity* 26(4): 473–492.

Koutavas A, DeMenocal PB, Olive GC et al. (2006) Mid-Holocene El Niño–Southern Oscillation (ENSO) attenuation revealed by individual foraminifera in eastern tropical Pacific sediments. *Geology* 34(12): 993–996.

Krzanowski A (1985) Implicaciones demográficas del patrón de asentamiento prehispánico en los Andes. El caso del valle Alto Chicama, Perú. *Journal de la Société des Americanistes* 71: 79–96.

Kus JS (1975) *Selected aspects of irrigated agriculture in the Chimu heartland, Peru*. Unpublished doctoral dissertation thesis, University of California, Los Angeles, CA.

Kus JS (1989) The sugar cane industry of the Chicama Valley, Peru. *Revista Geográfica* 109: 57–71.

Lachniet MS, Burns SJ, Piperno DR et al. (2004) A 1500-year El Niño/Southern Oscillation and rainfall history for the isthmus of Panama from speleothem calcite. *Journal of Geophysical Research: Atmospheres* 109(D20): 148–227.

Lagos P, Silva Y, Nickl E et al. (2008) El Niño – Related precipitation variability in Perú. *Advances in Geosciences* 14: 231–237.

Leonard B and Glenn R (1992) Informe Preliminar: Proyecto Reconocimiento Arqueológico Del Chicama, Resultados De La Primera Temporada De Campo, 1989, Trujillo, Peru.

Linsley RK Jr, Kohler MA and Paulhus JL (1988) *Hydrology for Engineers*. New York, NY: McGraw-Hill.

Manners RB, Magilligan FJ and Goldstein PS (2007) Floodplain development, El Niño, and cultural consequences in a hyperarid Andean environment. *Annals of the Association of American Geographers* 97(2): 229–249.

McMichael CH, Palace MW, Bush MB et al. (2014) Predicting pre-Columbian anthropogenic soils in Amazonia. *Proceedings of the Royal Society B: Biological Sciences* 281(1777): 20132475.

Moseley ME, Donnan CB, Keefer DK et al. (2008) Convergent catastrophe and the demise of Dos Cabezas: Environmental change and regime change in ancient Peru. In: Bourget S and Jones KL (eds) *The Art and Archaeology of the Moche: An Ancient Andean Society of the Peruvian North Coast*. Austin, TX: University of Texas Press, pp.81–92.

Moy CM, Seltzer GO, Rodbell DT et al. (2002) Variability of El Niño/Southern Oscillation activity at millennial timescales during the Holocene epoch. *Nature* 420: 162–165.

Nesbitt J (2016) El Niño and second-millennium BC monument building at Huaca Cortada (Moche Valley, Peru). *Antiquity* 90(351): 638–653.

Netherly PJ (1984) The management of late Andean irrigation systems on the north coast of Peru. *American Antiquity* 49: 227–254.

Ñiquen M and Bouchon M (2004) Impact of El Niño events on pelagic fisheries in Peruvian waters. *Deep Sea Research Part II Topical Studies in Oceanography* 51(6–9): 563–574.

ONERN (1973) *Inventario, Evaluacion y Uso Rational de Los Recursos Naturalies de La Costa: Cuenca Del Rio Chicama*. Lima, Peru: Oficina Nacional de Evaluacion de Recursos Naturales.

Orlove BS, Chiang JC and Cane MA (2000) Forecasting Andean rainfall and crop yield from the influence of El Nino on Pleiades visibility. *Nature* 403(6765): 68–71.

Ortlieb L (2000) The documented historical record of El Nino events in Peru: An update of the Quinn record (sixteenth through nineteenth centuries). In: Diaz H and Markgraf V (eds) *El Niño and the Southern Oscillation: Multiscale Vvariability and Gglobal and Rregional Iimpacts*. Cambridge: Cambridge University Press, pp.207–295.

Ortloff CR, Moseley ME and Feldman RA (1982) Hydraulic engineering aspects of the Chimu Chicama-Moche intervalley canal. *American Antiquity* 47: 572–595.

Phillips SJ, Anderson RP and Schapire RE (2006) Maximum entropy modeling of species geographic distributions. *Ecological Modelling* 190(3–4): 231–259.

Quinn WH, Neal VT and Antunez De Mayolo SE (1987) El Niño occurrences over the past four and a half centuries. *Journal of Geophysical Research: Oceans* 92(C13): 14449–14461.

Ramankutty N, Foley JA, Norman J et al. (2002) The global distribution of cultivable lands: Current patterns and sensitivity to possible climate change. *Global Ecology and Biogeography* 11(5): 377–392.

Ramírez IJ and Briones F (2017) Understanding the El Niño costero of 2017: The definition problem and challenges of climate forecasting and disaster responses. *International Journal of Disaster Risk Science* 8(4): 489–492.

Rasmusson EM and Wallace JM (1983) Meteorological aspects of the El Nino/southern oscillation. *Science* 222(4629): 1195–1202.

Richter M (2005) Vegetation development before, during, and after El Niño 1997/98 in northwestern Perú. *Lyonia* 8(2): 19–27.

Rodríguez R, Mabres A, Luckman B et al. (2005) "El Niño" events recorded in dry-forest species of the lowlands of northwest Peru. *Dendrochronologia* 22(3): 181–186.

Rollins HB, Richardson JB and Sandweiss DH (1986) The birth of El Niño: Geoarchaeological evidence and implications. *Geoarchaeology* 1(1): 3–15.

Sandweiss DH, Andrus CF, Kelley AR et al. (2020) Archaeological climate proxies and the complexities of reconstructing Holocene El Niño in coastal Peru. *Proceedings of the National Academy of Sciences* 117(15): 8271–8279.

Sandweiss DH, Maasch KA, Andrus CFT et al. (2007) Mid-Holocene climate and culture change in coastal Peru. In: Anderson DG, Maasch KA, Sandweiss DH et al. (eds) *Climate Change and Cultural Dynamics: A Global Perspective on Mid-Holocene Transitions*. New York, Boston, Paris: Elsevier/Academic Press, pp.25–50.

Sandweiss DH and Quilter J (2008) *El Niño, Catastrophism, and Culture Change in Ancient America*. Washington, DC: Dumbarton Oaks Pub Service.

Santana-Sagredo F, Dufour E, Goepfert N et al. (2020) New bioarchaeological evidence and radiocarbon dates from the Lambayeque/Sicán culture camelids from the El Brujo Complex (Northern coast of Peru): Implications for funerary and herd management practices. *Environmental Archaeology* 25(3): 333–352.

Schaedel RP (1988) *Andean World View: Hierarchy or Reciprocity, Regulation or Control? Current Anthropology*, vol. 29. Chicago, IL: University of Chicago Press, pp.768–775.

SENAMHI (2019) *Datos Hidrometeorológicos*. Lima, Peru: Servicio Nacional de Meteorologia e Hidrologia.

Shimada I, Schaaf CB, Thompson LG et al. (1991) Cultural impacts of severe droughts in the prehistoric Andes: Application of a 1,500-year ice core precipitation record. *World Archaeology: Archaeology and Arid Environments* 22(3): 247–270.

Shoji K (2018) La utilización de recursos malacológicos en el período Arcaico: Una perspectiva del sitio arqueológico Cruz Verde, Valle Chicama. *Archaeobios. Centro de Investigaciones Arqueobiológicas y Paleoecológicas Andinas* 12: 18–37.

Steiger NJ, Smerdon JE, Cook ER et al. (2018) A reconstruction of global hydroclimate and dynamical variables over the Common Era. *Scientific Data* 5(1): 180086.

Steiger NJ, Smerdon JE, Seager R et al. (2021) ENSO-driven coupled megadroughts in North and South America over the last millennium. *Nature Geoscience* 14(10): 739–744.

Tapley TD and Waylen PR (1990) Spatial variability of annual precipitation and ENSO events in western Peru. *Hydrological Sciences Journal* 35(4): 429–446.

Thompson LG, Henderson KA, Mosley-Thompson E et al. (2000) The tropical ice core record of ENSO. In: Diaz HF and Markgraf V (eds) *El Niño and the Southern Oscillation, Multiscale Variability and Global and Regional Impacts*. Cambridge: Cambridge University Press, pp.325–356.

Thompson LG, Mosley-Thompson E and Arnao BM (1984) El Nino-Southern Oscillation events recorded in the stratigraphy of the Tropical Quelccaya Ice Cap, Peru. *Science* 226(4670): 50–53.

Thompson LG, Mosley-Thompson E, Davis ME et al. (2011) Tropical glaciers, recorders and indicators of climate change, are disappearing globally. *Annals of Glaciology* 52(59): 23–34.

Thompson LG, Mosley-Thompson E, Davis ME et al. (2013) Annually resolved ice core records of tropical climate variability over the past~ 1800 years. *Science* 340(6135): 945–950.

Thompson LG, Mosley-Thompson E and Thompson PA (1992) Reconstructing interannual climate variability from tropical and subtropical ice-core records. In: Diaz HF and Markgraf V (eds) *El Niño: Historical and Paleoclimatic Aspects of the Southern Oscillation*. Cambridge: Cambridge University Press, pp.295–322.

Timmermann A, Oberhuber J, Bacher A et al. (1999) Increased El Niño frequency in a climate model forced by future greenhouse warming. *Nature* 398(6729): 694–697.

Toshihara K (2002) *The Cupisnique culture in the Formative period world of the Central Andes, Peru*. Urbana-Champaign: University of Illinois.

Tovar C, Sánchez Infantas E and Teixeira Roth V (2018) Plant community dynamics of lomas fog oasis of central Peru after the extreme precipitation caused by the 1997-98 El Niño event. *PLoS One* 13(1): e0190572.

Trenberth K (2021) NINO SST INDICES (NINO 1+2, 3, 3.4, 4; ONI AND TNI). The Climate Data Guide: Nino SST Indices (Nino 1+2, 3, 3.4, 4; ONI and TNI). Available at: https://climatedataguide.ucar.edu/climate-data/nino-sst-indices-nino-12-3-34-4-oni-and-tni

Trenberth KE and Hoar TJ (1997) El Niño and climate change. *Geophysical Research Letters* 24(23): 3057–3060.

Trouet V and Van Oldenborgh GJ (2013) KNMI Climate Explorer: A web-based research tool for high-resolution paleoclimatology. *Tree-Ring Research* 69(1): 3–13.

Vining B and Burns S (2018) Understanding the ecological decision-making of Tiwanaku pastoralists through geospatial agent-based models. In: Anemone R and Conroy G (eds) *New Geospatial Approaches to the Anthropological Sciences*. Albuquerque: UNM Press, pp.137–170.

Vining BR (2018) Cultural niche construction and remote sensing of ancient anthropogenic environmental change in the north coast of Peru. *Journal of Archaeological Method and Theory* 25: 559–586.

Vining BR, Hillman A and Contreras DA (2022) El Niño Southern Oscillation and enhanced arid land vegetation productivity in NW South America. *Journal of Arid Environments* 198: 104695.

Vining BR, Steinman BA, Abbott MB et al. (2019) Paleoclimatic and archaeological evidence from Lake Suches for highland Andean refugia during the arid middle-Holocene. *The Holocene* 29(2): 328–344.

Vuille M, Bradley RS, Werner M et al. (2003) Modeling δ^{18}O in precipitation over the tropical Americas: 1. Interannual variability and climatic controls. *Journal of Geophysical Research Atmospheres* 108: 1–24.

Vuille M, Burns SJ, Taylor BL et al. (2012) A review of the South American monsoon history as recorded in stable isotopic proxies over the past two millennia. *Climate of the Past* 8(4): 1309–1321.

Vuille M and Keimig F (2004) Interannual variability of summertime convective cloudiness and precipitation in the central Andes derived from ISCCP-B3 data. *Journal of Climate* 17(17): 3334–3348.

Vuille M and Werner M (2005) Stable isotopes in precipitation recording South American summer monsoon and ENSO variability: Observations and model results. *Climate Dynamics* 25(4): 401–413.

Wang B, Luo X, Yang Y-M et al. (2019) Historical change of El Niño properties sheds light on future changes of extreme El Niño. *Proceedings of the National Academy of Sciences* 116(45): 22512–22517.

Ward PJ, Jongman B, Kummu M et al. (2014) Strong influence of El Niño Southern Oscillation on flood risk around the world. *Proceedings of the National Academy of Sciences* 111(44): 15659–15664.

Watson RP (1979) *Water control and land use on the arid north coast of Peru: prehispanic agricultural systems in the Chicama Valley*. Master's Thesis, University of Texas, Austin, TX.

Waylen PR and Caviedes CN (1986) El Niño and annual floods on the north Peruvian littoral. *Hydrology Journal* 89(1–2): 141–156.

Woodroffe CD, Beech MR and Gagan MK (2003) Mid-late Holocene El Niño variability in the equatorial Pacific from coral microatolls. *Geophysical Research Letters* 30(7): 10-1–10–4.

Yaworsky PM, Vernon KB, Spangler JD et al. (2020) Advancing predictive modeling in archaeology: An evaluation of regression and machine learning methods on the Grand Staircase-Escalante National Monument. *PLoS One* 15(10): e0239424.

Yeh S-W, Kug J-S, Dewitte B et al. (2009) El Niño in a changing climate. *Nature* 461(7263): 511–514.

Zhang T, Hoell A, Perlwitz J et al. (2019) Towards probabilistic multivariate ENSO monitoring. *Geophysical Research Letters* 46(17–18): 10532–10540.